ISSN 1560-8034, 1605-6582 (On-line), SPQEO, 2021. V. 24, N 3. P. 319-327.

Optoelectronics and optoelectronic devices

Simulation and characterization of planar high-efficiency back contact silicon solar cells

A.V. Sachenko[1], V.P. Kostylyov[1], R.M. Korkishko[1], V.M. Vlasiuk[1], I.O. Sokolovskyi[1], B.F. Dvernikov[1], V.V. Chernenko[1], M.A. Evstigneev[2]

[1]*V. Lashkaryov Institute of Semiconductor Physics, NAS of Ukraine*
45, prospect Nauky, 03680 Kyiv, Ukraine
[2]*Memorial University of Newfoundland, St. John's, NL, Canada*
E-mail: sach@isp.kiev.ua; viktorvlasiuk@gmail.com

Abstract. Short-circuit current, open-circuit voltage, and photoconversion efficiency of silicon high-efficiency solar cells with all back contact (BCSC) with planar surfaces have been calculated theoretically. In addition to the recombination channels usually considered in this kind of modeling, namely, radiative, Auger, Shockley–Read–Hall, and surface recombination, the model also takes into account the nonradiative trap-assisted exciton Auger recombination and recombination in the space charge region. It is ascertained that these two recombination mechanisms are essential in BCSCs in the maximum power operation regime. The model results are in good agreement with the experimental results from the literature.

Keywords: modeling, solar cells, silicon, space charge region recombination, quantum efficiency.

https://doi.org/10.15407/spqeo24.03.319
PACS 88.40.jj

Manuscript received 20.04.21; revised version received 17.06.21; accepted for publication 18.08.21; published online 26.08.21.

1. Introduction

The vast majority of silicon solar cells currently used have one or two textured surfaces [1]. This radically reduces reflection of light at the air-semiconductor interface. At the same time, there are non-textured silicon-based SCs, in which reduction of light reflection is achieved by applying antireflection coatings. A special niche is now occupied by silicon SCs with back contact (BCSC). Although they are also mostly textured, but the physical basis of their operation is somewhat different from that of the traditional SC design [2]. In particular, these SCs must have long lifetimes of non-equilibrium charge carriers (~1 ms), which brings them closer to traditional highly efficient textured silicon SCs with two-sided contacts. Second, the rate of surface recombination at the illuminated surface in these SCs should be low enough, which also brings them closer to highly efficient textured silicon SCs. A separate issue for these SCs is to describe the intrinsic quantum efficiency of the photocurrent in the long-wave absorption region. To date, it has not been studied thoroughly enough.

In this work, a theoretical modeling of the key characteristics of these BCSC is performed, which takes into account all known components of the effective lifetime in silicon and the peculiarities of the internal quantum efficiency of photocurrent in the long-wave absorption region. The obtained theoretical curves have been compared to the experimental work [3], and a good agreement between the theory and experiment is achieved.

2. Effective recombination time in silicon

The general expression for the effective recombination lifetime in Si with the *n*-type base has the form

$$\tau_{eff}(n)=\left[\begin{array}{l}\dfrac{1}{\tau_{\rm SRH}(n)}+\dfrac{1}{\tau_{exc-{\rm Auger}}(n)}+\dfrac{S_{S0}}{d}\left(1+\dfrac{\Delta n}{n_0}\right)+\\ +\dfrac{1}{\tau_r(n)}+\dfrac{1}{\tau_{\rm Auger}(n)}+\dfrac{S_{SC}(n)}{d}\end{array}\right]^{-1}, \quad (1)$$

where $n = n_0 + \Delta n$ is the total majority carrier concentration, consisting of the equilibrium, n_0, and excess, Δn, contributions; $\tau_{\rm SRH}$ is the Shockley–Read–Hall (SRH) lifetime; S_{S0} – net recombination velocity on the front and rear surfaces at a low injection level; $\tau_{exc-{\rm Auger}}(n)=\tau_{\rm SRH}\cdot n_x/n_0$ – exciton Auger recombination time with $n_x = 8.2\cdot10^{15}$ cm^{-3} [4]; τ_r – radiative recombination time, $\tau_{\rm Auger}$ – band-to-band Auger recombination time [5], and d – the base thickness of SC. SRH lifetime in an *n*-type base is given by

$$\tau_{\mathrm{SRH}}(n) \cong \frac{\tau_{p0}\left(n_0+\Delta n+n_1\right)+\tau_{n0}\left(p_1+\Delta n\right)}{n_0+\Delta n}, \qquad (2)$$

where $\tau_{p0}=\left(C_pN_t\right)^{-1}$ and $\tau_{n0}=\left(C_nN_t\right)^{-1}$ are electron and hole lifetimes, n_1 and p_1 – equilibrium electron and hole concentration values in the case when Fermi level is the same as the deep-impurity energy. Depending on the value of the latter energy, as well as the electron and hole capture cross-sections, SRH lifetime as a function of excess concentration may change between two extreme values and may increase, decrease, or remain constant with Δn. In what follows, we will assume that τ_{SRH} = const.

It is worthwhile to dwell on the question why most today's simulations do not take into account non-radiative exciton recombination. In our opinion, the answer is that it is masked by the SRH and surface recombination. Indeed, redefinition of the SRH time as $\tau^*_{\mathrm{SRH}}=\tau_{\mathrm{SRH}}/\left(1+n_0/n_x\right)$ and surface recombination velocity as $S^*=S_0+\left(S_0+dn_0/\left(\tau_{\mathrm{SRH}}\cdot n_x\right)\right)\Delta n/n_0$ renders introduction of the non-radiative exciton Auger recombination unnecessary. Note that for $n_0 = 4.9\cdot10^{15}$ cm^{-3}, the value of τ^*_{SRH} is smaller than τ_{SRH} by about 60%. It should be also noted that an expression for the effective lifetime in Si similar to the formula for τ^*_{SRH} was used in some previous work [6] with $n_x = 7.1\cdot10^{15}$ cm^{-3}.

The inverse radiative lifetime at T = 300 K is $1/\tau_r(n)=A\left(n_0+\Delta n\right)$ with the radiative recombination parameter

$$A=\int_0^\infty A\left(E_{ph}\right)dE_{ph},$$

$$A\left(E_{ph}\right)=\alpha\left(E_{ph}\right)\left(\frac{n_r\left(E_{ph}\right)E_{ph}}{\pi c\hbar^{3/2}n_i(T)}\right)^2\exp\left(-\frac{E_{ph}}{kT}\right), \qquad (3)$$

where both the absorption coefficient α and refractive index n_r depend on the photon energy E_{ph} as tabulated in [7]. In order to approximately take into account the bandgap narrowing effect [8] by the amount ΔE_g, the argument of the absorption coefficient was shifted by the size of bandgap narrowing energy (see [9]), *i.e.* $\alpha(E_{ph}) = \alpha_0(E_{ph} + \Delta E_g)$, where α_0 is the absorption coefficient from [10] at zero bandgap narrowing size.

Lifetime due to recombination in SCR τ_{SCR} is defined as

$$\tau_{SCR}=\frac{d}{S_{SC}}, \qquad (4)$$

where S_{SC} is the SCR recombination velocity.

In most materials used for the manufacture of silicon SCs, the dependences $\tau_{\mathrm{SRH}}(\Delta n)$ and $\tau_{eff}(\Delta n)$ in the region of $\Delta n \le 10^{15}$ cm^{-3} are saturated (see, for example, the works [4, 5]). At the same time, in the finished silicon textured SCs in this area there is a decrease in the value $\tau_{eff}(\Delta n)$ with a decrease Δn (see, for example, the works [11, 12]). What is the difference between these two cases? In crystalline silicon samples used for measuring $\tau_{eff}(\Delta n)$, there is no *p-n* junction. At both surfaces of the sample, bends of bands are symmetrical and usually have a slight depletion. In this case, recombination in SCR is absent. At the same time, in the case of SC, a *p-n* junction is necessarily present. In this case, the recombination in the near-surface SCR is significant.

The SCR recombination velocity is given by the general expression

$$S_{SC}(\Delta n)=\int_0^w\frac{(n_0+\Delta n)dx}{\left[\left(\left(n_0+\Delta n\right)e^{y(x)}+n_i(T)\exp\left(\frac{E_t}{kT}\right)\right)+b_r\left(\left(p_0+\Delta n\right)e^{-y(x)}+n_i(T)\exp\left(-\frac{E_t}{kT}\right)\right)\cdot\tau_R(x)\right]}. \qquad (5)$$

Here, the time of SCR recombination $\tau_R(x)$ is related to the concentration of traps, $N_t(x)$, as $\tau_R(x)=\left(V_p\sigma_pN_t(x)\right)^{-1}$, the ratio of the hole-to-electron capture rate constants $b_r=\left(V_p\sigma_p/V_n\sigma_n\right)$ is expressed in terms of the electron and hole thermal velocities and capture cross-sections, $V_{n,p}$ and $\sigma_{n,p}$. The trap energy E_t is measured from the middle of the bandgap, p_0 – equilibrium hole concentration, $n_i(T)$ – intrinsic charge carriers concentration, and w – SCR thickness. Finally, $y(x)$ is the electric potential normalized to the thermal voltage $k_{\mathrm{B}}T/q$.

To find the dependence of the non-dimensional potential $y(x)$ on the coordinate x, it is necessary to use the solution of the Poisson equation

$$x=\int_{y_0}^{y}\frac{L_{\mathrm{D}}}{\left[\left(1+\frac{\Delta n}{n_0}\right)\left(e^{y_1}-1\right)-y_1+\frac{\Delta n}{n_0}\left(e^{-y_1}-1\right)\right]^{0.5}}dy_1. \qquad (6)$$

where $L_{\mathrm{D}}=\left(\varepsilon_0\varepsilon_{\mathrm{Si}}kT/2q^2n_0\right)^{1/2}$ is the Debye length, q – elementary charge, ε_0 – vacuum permittivity, and $\varepsilon_{\mathrm{Si}}$ – dielectric constant of Si.

The initial value of the potential, $y_0 = y(x = 0)$, is found by modeling the n-p^+ junction on the p^+-side as a thin negatively charged slab with the surface charge density $-qN$, N being the surface concentration of acceptor ions in that slab. Then, from the Poisson equation, one can find

$$N = \pm\left(\frac{2kT\varepsilon_0\varepsilon_{Si}}{q^2}\right)^{1/2} \times \\ \times\left[(n_0+\Delta n)\left(e^{y_0}-1\right)-n_0y_0+\Delta n\left(e^{-y_0}-1\right)\right]^{1/2}. \quad (7)$$

From the equation (6), one can obtain the following expression for the SCR thickness w

$$w = \int_{y_0}^{y_w}\frac{L_D}{\left[\left(1+\frac{\Delta n}{n_0}\right)\left(e^{y}-1\right)-y+\frac{\Delta n}{n_0}\left(e^{-y}-1\right)\right]^{0.5}}dy, \quad (8)$$

where y_w is the non-equilibrium dimensionless potential at the SCR boundary with the quasi-neutral bulk.

Having the expressions (5)–(8), one can calculate the dependence of the quantity S_{SC} on the excess concentration of electron-hole pairs Δn.

As the analysis showed, in the approximation of the constant lifetime in SCR, taking into account the fact that $\tau_R << \tau_{SRH}$, the calculated dependences of the value $S_{SC}(\Delta n)$ are much more inclined than the experimental values, and agreement between theory and experiment is not achieved.

A much better agreement between the experiment and the theory can be obtained by assuming that the distribution of the inverse lifetime in SCR is described by Gaussian

$$\tau_R^{-1}(x) = \tau_m^{-1}\exp\left(\frac{-(x-x_m)^2}{2\sigma^2}\right), \quad (9)$$

where τ_m is the lifetime at the maximum point, x_m – position of the maximum, σ – dispersion.

In this case, a faster decline $S_{SC}(\Delta n)$ occurs by reducing the half-width of the Gaussian, and large enough values $S_{SC}(\Delta n)$ at small Δn can be achieved by reducing the lifetime τ_m.

As calculations showed, the value S_{SC} significantly depends on the value of the excess concentration of electron-hole pairs Δn. The smaller the value Δn, the larger the value S_{SC}. Another factor that determines the amplitude of S_{SC} is the SRH lifetime in SCR τ_m. The smaller its value, the larger the value S_{SC}. In direct bandgap semiconductors, where the SRH lifetime τ_{SRH} is small (see, for example, [13]), the value S_{SC} is sufficiently large and competes with the value of the recombination rate in the neutral bulk at those values Δn that are realized for SC in the maximum power operation regime. Therefore, when modeling their characteristics, recombination in SCR should be considered. Another situation is realized in high-performance silicon SC, in particular, in BCSC. Their SRH lifetime in the neutral bulk τ_{SRH} is of the order of or higher than 1 ms [11, 12]. If to assume that $\tau_m \propto \tau_{SRH}$, then, as estimates show, at voltages that are realized for SC in the maximum power operation regime, the value of $S_{SC} \le 10^{-2}$ cm/s and, at first glance, it can be neglected in comparison with other recombination components. But, as the analysis performed in [14, 15] showed, the main difference between recombination in SCR and recombination in the neutral bulk in the case of silicon is that the lifetime in SCR τ_m can be several orders of magnitude less than the SRH lifetime τ_{SRH}. For the cases analyzed in [14, 15], its value in the order of magnitude was 1 μs. This primarily indicates that the concentration of deep levels in SCR responsible for SRH recombination significantly exceeds the concentration of deep levels in the neutral bulk. The reasons for the increase in the concentration of deep levels in SCR, which lead to a decrease τ_m, may be due to the presence of effects of saturation during high-temperature diffusion to create a p-n junction, the presence of boron complexes, which increases the concentration of deep levels, with effects associated with high values of electric field in SCR and with other factors. In this regard, the area on the dependences of the dark recombination current on the voltage applied to silicon SC is determined by recombination in SCR, when the factor of non-ideality inherent to the I–V characteristics is close to two, not only in the region of sufficiently small V values (0.4 V). It can be realized up to the voltage values at the point of maximum power when $V = V_m$ (V_m = 0.55 – 0.65 V) (see [15]).

As a result, there is a situation when the recombination rate of SCR of highly efficient silicon SCs in the maximum power operation regime becomes comparable with other recombination components, which leads to the need to take into account recombination in SCR in modeling the characteristics of SCs.

3. Photoconversion parameters of BCSC

If the minority carriers' diffusion length $L_d = \sqrt{D_p\tau_{eff}}$ is much higher than one-quarter of the base thickness d/4, and if the combined surface and SCR recombination velocity $S_{SC} + S_{S0} << 2D_p/d$, then the excess concentration profile is practically uniform in the base region. In that case, one can employ the narrow-base approximation and express the I–V relation under illumination as [8]

$$I(V) = I_L - \frac{qA_{SC}d\,\Delta n}{\tau_{eff}} - \frac{V+IR_s}{R_{SH}}, \quad (10)$$

where the first term is the light-generated current, the second term – recombination current, A_{SC} – SC area, and R_S, R_{SH} are the series and shunt resistances, respectively.

The excess carrier concentration is related to the applied voltage by a modified acting mass law

$$(n_0+\Delta n)(p_0+\Delta n)=n_i^2\exp\left(\frac{\Delta E_g+q(V-IR_S)}{kT}\right), \quad (11)$$

where n_i is the intrinsic concentration at low injection [10], and $\Delta E_g(n_0, \Delta n)$ is the magnitude of bandgap narrowing in Si [9]. Eq. (11) can be solved for the excess concentration

$$\Delta n=-\frac{n_0}{2}+\sqrt{\frac{n_0^2}{4}+n_i^2e^{\Delta E_g/kT}\left(e^{q(V-IR_s)/kT}-1\right)}. \quad (12)$$

Equations (10)–(12) need to be solved numerically. The photoconversion efficiency η, as well as the voltage V_m, current I_m, and output power P_m in the maximum-power operation regime are found by setting the derivative of $P = IV$ with respect to voltage tending to zero. The open-circuit voltage and the short-circuit current are obtained by setting in (10) I and V equal to zero. The value of the excess concentration in the open-circuit mode Δn_{OC} when the condition $L_d >> d$ is met and $I_L >> V_{OC}/R_{SH}$ can be found from the balance equation taken in the form

$$I_L/q=A_{SC}\left[\frac{d}{\tau_{eff}(\Delta n_{OC})}\right]\Delta n_{OC}. \quad (13)$$

External quantum efficiency $EQE(\lambda)$ related to the internal quantum efficiency $IQE(\lambda)$ and reflection coefficient $R(\lambda)$ by

$$EQE(\lambda)=f\cdot IQE(\lambda)(1-R(\lambda)), \quad (16)$$

where the numerical coefficient $f < 1$ has to do with the fact that part of the incident radiation is absorbed by a coating layer outside of the semiconductor. The simple limit approximation for IQE of SC with specular flat surfaces when the reflection coefficient of the rear surface equal to 1 is

$$IQE(\lambda)=1-\exp(-2\alpha(\lambda)d). \quad (17)$$

A more accurate expression can be obtained by solving the stationary diffusion equation for the excess carrier concentration with the boundary conditions

$$j(x=0)=-S_0\Delta n(x=0), \quad \Delta p(x=d)=0, \quad (19)$$

where S_0 is the net recombination velocity on the front surface. The solution of this equation is

$$\Delta n=C_1e^{-\frac{x}{L}}+C_2e^{\frac{x}{L}}+\frac{\alpha I_0\tau}{1-(\alpha L)^2}\left[e^{-\alpha x}+R_de^{\alpha(-2d+x)}\right], \quad (18)$$

where R_d is the reflection coefficient of the rear surface, the integration constants $C_{1,2}$ are to be found from (19).

The internal quantum efficiency $IQE(\lambda) = j(x = d)$ then becomes

$$IQE(\lambda)=\frac{\alpha L}{1-\alpha^2L^2}\frac{-\left[(S_0L/D)\left(\left(1-R_de^{-2\alpha d}\right)-e^{-\alpha d-d/L}\left(1+R_d\right)\right)+\alpha L\left(1-R_de^{-2\alpha d}\right)+e^{-\alpha d-d/L}\left(1+R_d\right)\right]}{\cosh(d/L)+(S_0L/D)\sinh(d/L)}+$$
$$+\frac{\alpha L}{1-\alpha^2L^2}\left[\left(\left(1+R_d\right)+\alpha L\left(1-R_d\right)\right)e^{-\alpha d}\right]. \quad (20)$$

The expression for the dependence $V_{OC}(V)$ obtained using (12) is as follows

$$V_{OC}=\frac{kT}{q}\ln\left(\frac{\left(\Delta n_{OC}+\frac{n_0}{2}\right)^2-\frac{n_0^2}{4}}{n_{i0}(T)^2e^{\Delta E_g/kT}}+1\right)=$$
$$=\frac{kT}{q}\ln\left(\frac{(\Delta n_{OC}+n_0)\Delta n_{OC}}{n_{i0}(T)^2e^{\Delta E_g/kT}}+1\right). \quad (14)$$

4. Spectral dependences of the photocurrent of BCSC

In this approximation, the photocurrent generated by the light is a fitting parameter. On the other hand, it can be found by integrating the product of the incident photon flux with the spectral distribution $I(\lambda)$ by the external quantum efficiency SC $EQE(\lambda)$ as

$$J_L=q\int EQE(\lambda)I(\lambda)\,d\lambda. \quad (15)$$

Shown in Fig. 1 is the spectral dependence, if IQE is in accord with (15) (curve *1*) and (17) (curves *2*–*6*) for the special case $R_d = 1$. As seen in this figure, when $L = 1$ cm and $S_0 = 0$, (17) and (20) yield identical results.

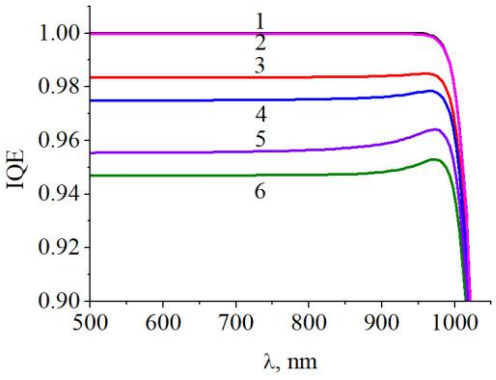

Fig. 1. Theoretical spectral dependences of internal quantum efficiency of BCSC for d = 300 μm, R_d = 1. L (in μm) and S_0 (in cm/s): 10^4, 0 (*2*); 1640, 0 (*3*); 1640, 3 (*4*); 1640, 10 (*5*); 900, 0 (*6*). *IQE* is in accord with Eq. (15) (curve *1*).

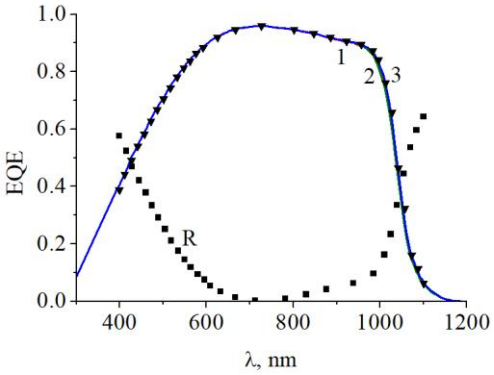

Fig. 2. Experimental spectral dependences of *EQE* and *R* (squares) of BCSC.

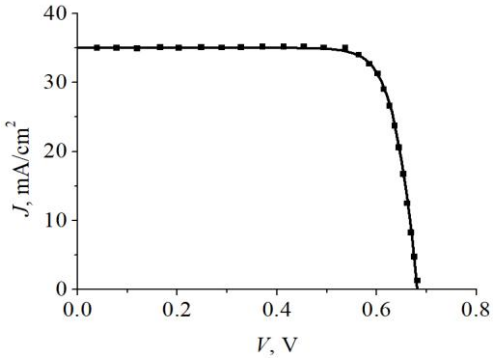

Fig. 4. Experimental (symbols) and theoretical (solid line) *I–V* curve for BCSC under illuminatation.

Upon decreasing *L*, the maximal *IQE* values get smaller (see curves *3* and *6*). Likewise, increasing S_0 also results in the smaller *IQE* maxima (curves *4* and *5*).

Fig. 2 shows the experimental *EQE*(λ) and *R*(λ) curves for BCSC from [3], as well as the theoretical approximations (17), (20) for d = 300 μm, L = 0.17 cm, and S_0 = 3 cm/s. The value of R_d was also slightly varied. As seen in the figure, the theoretical *EQE*(λ) curve agrees with the experimental one very well.

Once *EQE*(*λ*) is known, the dependence of the light-generated photocurrent on the base thickness *d* follows immediately, see (17), allowing us to optimize SC with respect to the base thickness.

5. Results and discussion

We first analyze the results obtained in [3] for BCSC with the photoconversion efficiency 19.2%. To model its key parameters, it is necessary to determine the recombination parameters τ_R and b_r from the measurements of dark *I–V* curves. In addition, it is necessary to find the SRH lifetime and surface recombination velocity. Fig. 3 shows the experimental dependences of the dark current density for the studied SCs on the applied voltage at the temperature 25 °C,

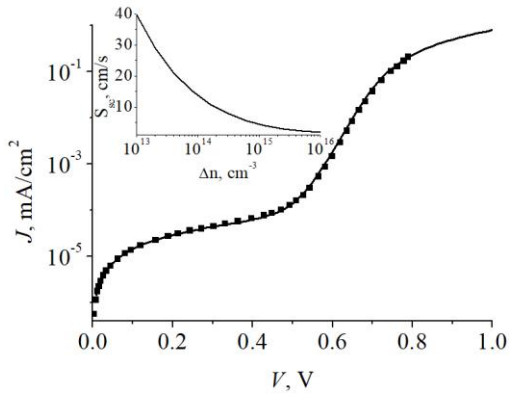

Fig. 3. Experimental (symbols) and theoretical (solid line) dark *I–V* curves. The insert shows a theoretical relationship $S_{SC}(\Delta n)$.

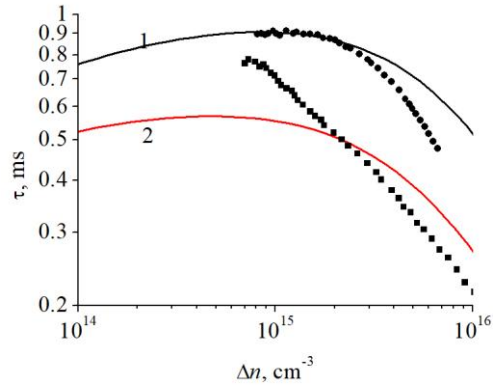

Fig. 5. Experimental (symbols) and theoretical (solid lines) bulk (*1*) and effective (*2*) lifetimes *vs* excess concentration.

while Fig. 4 shows the experimental dependences for the light generated current density as a function of the applied voltage under the AM1.5 conditions. The dependence $S_{SC}(\Delta n)$ at the above parameters is based on the insert in Fig. 3.

Fig. 5 shows the experimental effective and bulk lifetimes for the freshly formed SCs (before metallization) on the excess concentration of charge carriers. Finally, Fig. 6 shows the experimental dependences of the light intensity on the open-circuit voltage for the solar spectrum corresponding to the conditions AM1.5.

The SRH lifetime τ_{SRH} can be determined from the fit of the experimental bulk lifetime *vs* the excess concentration $\tau_b(\Delta n)$ curve shown in Fig. 5. Given that its maximum is at $\Delta n = 10^{15}$ cm^{-3}, τ_{SRH} can be found from the magnitude of τ_b equal to $2.1 \cdot 10^{-3}$ s. The values of τ_m, x_m, σ and b_r are found from fitting the experimental dependences dark current *vs* voltage curve, whereas S_{S0} can be found by fitting the *I–V* curve in the presence of illumination. The value of the series resistance was determined by fitting the experimental and theoretical values photoconversion efficiency and proved to be equal to 0.64 Ohm·cm^2.

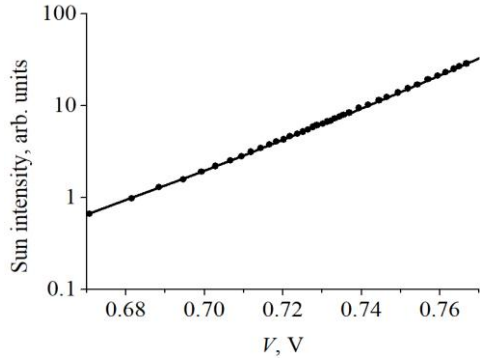

Fig. 6. Experimental (points) and theoretical (line) dependences of illuminance *vs* open-circuit voltage.

NN	1	2	3	4
$V_{OC\,exp}$, mV	683.2	681.4	682.5	682.0
$V_{OC\,theor}$, mV	683.2	681.4	682.5	682.0
FF_{exp}, %	78.2	80.4	79.4	80.5
FF_{theor}, %	78.2	80.4	79.4	80.5
η_{exp}, %	18.7	19.1	18.9	19.2
η_{theor}, %	18.7	19.1	18.9	19.2
S_{S0}, cm/s	15.7	18.2	16.6	17.4
$R_{S\,exp}$, Ohm·cm^2	1.3	0.9	1.1	0.8
$R_{S\,theor}$, Ohm·cm^2	1.09	0.67	0.74	0.64
$R_{S1\,theor}$, Ohm·cm^2	1.03	0.65	0.71	0.63

A good fit is achieved by using the following parameters: $\tau_m = 3.8\cdot10^{-6}$ s, $x_m = 8.5\cdot10^{-6}$ cm, $b_r = 0.1$, $\sigma = 2.4\cdot10^{-6}$ cm, $\tau_{SRH} = 2.1\cdot10^{-3}$ s, S_{S0} =17.4 cm/s, $R_S = 0.64$ Ohm·cm^2.

As can be seen from Figs 3 and 4, the theoretical dark and illuminated *I–V* curves agree well with the experimental ones.

With the above parameters, one can also plot the theoretical curve for effective lifetime as a function of Δn, shown in Fig. 5. As can be seen from this figure, in the region $\Delta n < 10^{15}$ cm^{-3}, the effective lifetime decreases with decreasing Δn. This decline is associated with the recombination in SCR. Incidentally, the point of maximum power in this case happens to be $1.96\cdot10^{14}$ cm^{-3}, and the effective lifetime at this point is $5.6\cdot10^{-4}$ s. When $\Delta n = 1.96\cdot10^{14}$ cm^{-3}, the value $S_{SC} = 9.7$ cm/s, and the value S_S is 18.1 cm/s, *i.e.*, they are commensurate with each other.

Unfortunately, the dependences of $\tau_b(\Delta n)$ and $\tau_{eff}(\Delta n)$ shown in Fig. 5 are given not for the case of SC, but for the material from which this SC is made. To obtain the correct dependence of $\tau_{eff}(\Delta n)$, which takes place for the studied SC, one needs to use the dependence of illuminance *vs* the open-circuit voltage shown in Fig. 6.

To do this, the expression (13) should be used, which should replace J_L by illumination for the case of the solar spectrum under conditions AM1.5. The dependence of $\tau_{eff}(\Delta n)$ obtained using the above parameters is shown in Fig. 5. The same figure shows the dependence of $\tau_b(\Delta n)$ calculated using expressions for different components of recombination time. As can be seen from the figure, the values of $\tau_{eff}(\Delta n)$ and $\tau_b(\Delta n)$ differ for the cases of material and SC. From the constructed dependence $\tau_{eff}(\Delta n)$, it is seen that, in the region $\Delta n < 10^{15}$ cm^{-3}, the descending section is realized. This decline is associated with recombination in SCR.

With the above parameters, the open-circuit voltage calculated using the experimental value of the short-circuit current density of 35 mA/cm^2 is 682 mV, which is completely identical to the experimental value. The calculation of the photoconversion efficiency using the approach described above with the above parameters and the value of the series resistance of 0.64 Ohm·cm^2 gives a value of 19.2%, which also coincides with the experimental value. With the theoretical values of V_m and J_m, the fill factor equals 0.805, which coincides with the experimental value [3].

In the same way, the key parameters of the other three SCs can be calculated. A comparison of the experimental (see Table 1 of [3]) and theoretical parameter values is given in Table.

In addition to the key parameters of SCs, Table shows the value of S_{S0} and of the series resistance calculated in two approximations. In the first approximation, R_S was obtained from fitting the experimental and theoretical photoconversion efficiency curves (see the penultimate column in Table). In the second approach (the last column in Table), the values of the series resistance were calculated as

$$R_{s1} = \left(1 - \frac{\eta}{\eta(R_s = 0)}\right)\frac{V_m}{J_m} \equiv \left(1 - \frac{FF}{FF(R_s = 0)}\right)\frac{V_m}{J_m} \ . \qquad (21)$$

As seen from Table, the theoretical values of the key parameters agree with the experimental ones with the accuracy better than 0.1%, which significantly exceeds the experimental error. With respect to the experimental and calculated series resistance values, the differences are much larger. The smallest discrepancy between the two theoretical methods above is about 3%. The biggest difference between the theoretical and experimental R_S values from Table is about 40%.

In [3], the method of measuring the series resistance is not explained. Usually, the method of two intensities is used for this purpose. This method does not take into account the corrections associated with the bandgap narrowing, which should lead to an increase in the series resistance value. Note also that Eq. (21) is approximate, whereas the most accurate value of R_S is found by fitting the experimental photoconversion efficiency results.

Table also shows the low-signal values of surface recombination velocity S_{S0} in different SCs. As can be seen from Table, there is a clear correlation between the open-circuit voltage and the values of S_{S0}, namely: the lower S_{S0}, the higher the value of the open-circuit voltage.

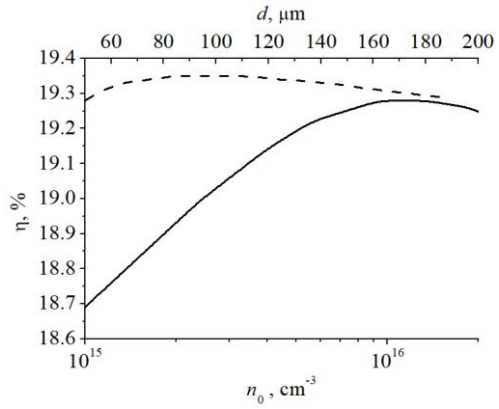

Fig. 7. Theoretical photoconversion efficiency *vs* doping level (solid line) and the base thickness (dashed line).

Shown in Fig. 7 solid line demonstrates the theoretical photoconversion efficiency *vs* the base doping level curves for SCs with the efficiency close to 19.2%. As can be seen from the figure, the maximum of the photoconversion efficiency close to 19.3% is realized at the level of base doping $1.2 \cdot 10^{16}$ cm^{-3} The efficiency value at $n_0 = 4.9 \cdot 10^{15}$ cm^{-3} is lower than the maximum one by 1%-rel.

Fig. 7 shows also the theoretical dependences of the photoconversion efficiency for SCs with $\eta_{exp} = 19.2\%$ as a function of the base thickness (dashed line). As can be seen from the figure, the maximum efficiency occurs at the base thickness close to 95 μm. The relative difference between the maximal value and the value at the base thickness of 300 μm is 1%.

Thus, this approach allows both to theoretically describe the key parameters of the high-performance silicon SCs with flat surfaces, and to obtain optimal values of their thickness and doping level.

6. Conclusions

The performance of silicon SCs with a flat surface [3] has been analyzed within the thin base approximation. It has been shown that near the absorption edge, their internal quantum efficiency is described as $1–e^{-2\alpha(\lambda)d}$. The calculations take into account all known recombination mechanisms in silicon, namely: Shockley–Read–Hall recombination, surface recombination, recombination in SCR, radiative recombination, nonradiative excitonic trap-assisted Auger recombination, and band-to-band Auger recombination. An important parameter has been determined: the recombination lifetime in SCR. It has been shown that including the nonradiative exciton recombination into consideration is equivalent to the renormalization of the SRH lifetime. The difference between the true and the effective SRH lifetimes increases with the doping concentration. The proposed approach allowed calculating the key photovoltaic parameters: short-circuit current density, open-circuit voltage, as well as the fill factor and photoconversion efficiency. A comparison of the theoretical results with the experimental curves for the four SC samples from [1] showed almost perfect agreement and allowed calculating optimal values of the doping level and thicknesses for those SCs.

Acknowledgment

This work was partially supported (V. Kostylyov and V. Vlasiuk) by National Research Foundation of Ukraine by the state budget finance (project 2020.02/0036 “Development of physical base of both acoustically controlled modification and machine learning–oriented characterization for silicon solar cells”).

References

1. Green M.A. *Third Generation Photovoltaics. Advanced Solar Energy Conversion*. Springer, 2006.
2. Sachenko A.V., Gorban A.P., Kostylyov V.P., Serba A.A., Sokolovskyi I.O. Comparative analysis of photoconversion efficiency in the Si solar cells under concentrated illumination for the standard and rear geometries of arrangement of contacts. *Semiconductors.* 2007. **41**, No 10. P. 1214–1223. https://doi.org/10.1134/S106378260710017X.
3. Zin N., Blakers A., McIntosh K. *et al.* 19% Efficient *n*-type all-back-contact silicon wafer solar cells with planar front surface. *Proc. 49th Australian Solar Energy Society’s (AuSES) Conf.*, Sydney, Australia, Nov. 30 – Dec. 2, 2011.
4. Sachenko A.V., Kostylyov V.P., Vlasyuk V.M. *et al.* The influence of the exciton nonradiative recombination in silicon on the photoconversion efficiency. *Proc. 32 European Photovoltaic Solar Energy Conf. and Exhib*., Munich, Germany, 20–24 June 2016. P. 141–147. https://doi.org/10.4229/EUPVSEC20162016-1BV.5.14.
5. Richter A., Glunz S., Werner F. *et al.* Improved quantitative description of Auger recombination in crystalline silicon. *Phys. Rev. B.* 2012. **86**. P. 165202: 1–14. https://doi.org/10.1103/PhysRevB.86.165202.
6. Fossum J.G. Computer-aided numerical analysis of silicon solar cells. *Solid State Electron.* 1976. **19**, No 4. P. 269–277. https://doi.org/10.1016/0038-1101(76)90022-8.
7. Green M.A. Self-consistent optical parameters of intrinsic silicon at 300 K including temperature coefficients. *Solar Energy Materials and Solar Cells.* 2008. **92**. P. 1305–1310. https://doi.org/10.1016/j.solmat.2008.06.009.
8. Sachenko A., Kostylyov V., Sokolovskyi I., and Evstigneev M. Effect of temperature on limit photoconversion efficiency in silicon solar cells. *IEEE J. Photovolt.* 2020. **10**. P. 63–69. https://doi.org/10.1109/JPHOTOV.2019.2949418.
9. Schenk A. Finite-temperature full random-phase approximation mode of band gap narrowing for silicon device simulation. *J. Appl. Phys.* 1998. **84**, No 7. P. 3684–3695. https://doi.org/10.1063/1.368545.

10. Trupke T., Green M.A., Würfel P. *et al.* Temperature dependence of the radiative recombination coefficient of intrinsic crystalline silicon. *J. Appl. Phys.* 2003. **94**, No 8. P. 4930–4937. https://doi.org/10.1063/1.1610231.
11. Sachenko A.V., Kostylyov V.P., Kulish N.R. *et al.* Model of efficiency of multijunction solar cell. *Semiconductors.* 2014. **48**, No 5. P. 675–682. https://doi.org/10.1134/S1063782614050182.
12. Yoshikawa K., Yoshida W., Irie T. *et al.* Exceeding conversion efficiency of 26% by heterojunction interdigitated back contact solar cell with thin film Si technology. *Solar Energy Materials and Solar Cells.* 2017. **173**. P. 37–42. https://doi.org/10.1016/j.solmat.2017.06.024.
13. Richter A., Benick J., Feldmann F. *et al. n*-Type Si solar cells with passivating electron contact: Identifying sources for efficiency limitations by wafer thickness and resistivity variation. *Solar Energy Materials and Solar Cells.* 2017. **173**. P. 96–105. https://doi.org/10.1016/j.solmat.2017.05.042.
14. Sachenko A.V., Kostylyov V.P., Vlasiuk V.M. *et al.* Features in the formation of a recombination current in the space charge region of silicon solar cells. *Ukr. J. Phys.* 2016. **61**, No 10. P. 917–922. https://doi.org/10.15407/ujpe61.10.0917.
15. Sachenko A.V., Kostylyov V.P., Sokolovskyi I.O. *et al.* Specific features of current flow in α-Si: H/Si heterojunction solar cells. *Techn. Phys. Lett.* 2017. **43**, No 2. P. 152–155. https://doi.org/10.1134/S1063785017020109.

Authors and CV

Sachenko A.V. Professor, Doctor of Sciences (Phys & Math), Chief Researcher of the Laboratory of Physical and Technical Fundamentals of Semiconductor Photovoltaics at the V. Lashkaryov Institute of Semiconductor Physics. He is the author of more than 300 scientific publications. His main research interests include analysis, characterization, and modeling of silicon solar cells.
https://orcid.org/0000-0003-0170-7625

Vlasiuk V.M. PhD, Researcher of the Laboratory of Physical and Technical Fundamentals of Semiconductor Photovoltaics, V. Lashkaryov Institute of Semiconductor Physics. He is the author of more than 35 scientific publications. The area of his scientific interests includes research, analysis of silicon solar cells. https://orcid. org/0000-0001-6352-0423

Kostylyov V.P. Professor, Doctor of Sciences (Phys & Math), Head of the Laboratory of Physical and Technical Fundamentals of Semiconductor Photovoltaics at the V. Lashkaryov Institute of Semiconductor Physics. He is the author of more than 250 scientific publications. The area of his scientific interests includes photovoltaics and betavoltaics, research, analysis and modelling of solar cells, testing the solar cells, characterization and metrology as well as characterization of the optical and recombination properties of photovoltaics materials.
https://orcid.org/0000-0002-1800-9471;
vkostylyov@ukr.net

Korkishko R.M. PhD, Researcher of the Laboratory of Physical and Technical Fundamentals of Semiconductor Photovoltaics at the V. Lashkaryov Institute of Semiconductor Physics. He is the author of more than 46 scientific publications. The area of his scientific interests includes research, analysis of silicon solar cells.
romkin.ua@gmail.com;
https://orcid.org/0000-0002-4568-574X

Sokolovskyi I.O. PhD, Senior Researcher of the Laboratory of Physical and Technical Fundamentals of Semiconductor Photovoltaics at the V. Lashkaryov Institute of Semiconductor Physics. He is the author of more than 70 scientific publications. His main research interests include modeling of silicon solar cells.
https://orcid.org/0000-0002-7072-6670;
i.o.sokolovskyi@gmail.com

Chernenko V.V. Senior Researcher of the Laboratory of Physical and Technical Fundamentals of Semiconductor Photovoltaics at the V. Lashkaryov Institute of Semiconductor Physics. He is the author of more than 100 scientific publications. His main research interests include research, analysis of silicon solar cells.
https://orcid.org/0000-0002-7630-6925;
vvch@isp.kiev.ua

Dvernikov B.F. Researcher of the Laboratory of Physical and Technical Fundamentals of Semiconductor Photovoltaics, V. Lashkaryov Institute of Semiconductor Physics. The area of his scientific interests includes manufacturing the equipment for silicon solar cells testing.
https://orcid.org/0000-0003-2917-8948;
dvernikov@isp.kiev.ua

Evstigneev M.A. Assistant Professor of the faculty of Physics and Physical Oceanography at the Memorial University of Newfoundland. His research areas are non-equilibrium statistical physics, biophysics, surface science.

https://orcid.org/0000-0002-7056-2573;
mevstigneev@mun.ca

Симуляція та характеризація планарних високоефективних сонячних елементів із тильним контактом

А.В. Саченко, В.П. Костильов, Р.М. Коркішко, В.М. Власюк, І.О. Соколовський, Б.Ф. Дверніков, В.В. Черненко, М. Євстігнєєв

Анотація. У роботі змодельовано ключові параметри кремнієвих високоефективних сонячних елементів з тильною металізацією (СЕТМ) з плоскими поверхнями, такі, зокрема, як струм короткого замикання, напруга розімкненого кола та ефективність фотоперетворення. При моделюванні додатково враховано такі рекомбінаційні механізми, як безвипромінювальна екситонна рекомбінація за механізмом Оже за участю глибокого рекомбінаційного рівня та рекомбінація в області просторового заряду. Встановлено, що вони істотні для досліджених СЕТМ в режимі відбору максимальної потужності. Результати моделювання добре узгоджуються з експериментальними даними з літератури.

Ключові слова: моделювання, сонячний елемент, кремній, рекомбінація в області просторового заряду, квантова ефективність.